Competition between delamination and tearing in multiple peeling problems

Competition between delamination and tearing in multiple peeling problems

Lucas Brely[(1)], Federico Bosia[(1)], Stefania Palumbo [(2)], Massimiliano Fraldi[(2)], Ali Dhinojwala[(3)] and Nicola M. Pugno[(4,5,6)*]

(1) Department of Physics and "Nanostructured Interfaces and Surfaces" Inter-Departmental Centre, Università di Torino, Via P. Giuria 1, 10125, Torino (Italy).

(2) Department of Structures for Engineering and Architecture, University of Napoli Federico II, Italy

(3) Department of Polymer Science, The University of Akron, Akron, Ohio 44325-3909

(4) Laboratory of Bio-Inspired & Graphene Nanomechanics, Department of Civil, Environmental and Mechanical Engineering, Università di Trento, via Mesiano, 77, I-38123 Trento, Italy.

(5) School of Engineering and Materials Science, Queen Mary University of London, Mile End Road, London E1 4NS, UK.

(6) Fondazione E. Amaldi, Ket Lab, Via del Politecnico snc, 00133 Rome, Italy.

(*) Corresponding author: *nicola.pugno@unitn.it*

Keywords: Adhesion, fracture, multiple peeling, Simulations, Spider web

Abstract

Adhesive attachment systems consisting of multiple tapes or strands are commonly found in nature, for example in spider web anchorages or in mussel byssal threads, and their structure has been found to be ingeniously architected in order to optimize mechanical properties, in particular to maximize dissipated energy before full detachment. These properties emerge from the complex interplay between mechanical and geometric parameters, including tape stiffness, adhesive energy, attached and detached lengths and peeling angles, which determine the occurrence of three main mechanisms: elastic deformation, interface delamination and tape fracture. In this paper, we introduce a formalism to evaluate the mechanical performance of multiple tape attachments in different parameter ranges, prediction of the corresponding detachment behaviour. We also introduce a numerical model to simulate the multiple peeling behaviour of complex structures, illustrating its predictions in the case of the staple-pin architecture. We expect the presented formalism and the numerical model might provide important tools for the design of bioinspired adhesive systems with tuneable or optimized detachment properties.

1. Introduction

Spider silk is a biological fibrous material that displays exceptional mechanical properties [1] and comes in many different types, each with specific functions and properties [2]. Silk is the base construction material of spiders, and is used to fabricate complex structures such as the spider web. In addition to the main structure, the attachment between the silk threads and the substrate (Fig.1a) plays an important role in determining the functionality of silk-based architectures. For example, it was shown that the contact, usually performed through adhesive-coated “silken” threads called “attachment discs” [3] differs in geometrical features depending on its prey-capture or locomotion functions [4]. To create a safe attachment between the dragline and the substrate, spiders create a

structure referred to as a “staple-pin” attachment. An array of perpendicular silken threads are used to “coat” the main thread on which the external load is applied (see Fig. 1a) [5]. When staple-pin structures are subjected to a peel test, different types of behaviour have been observed in natural systems [6]. The detachment occurs in some cases by delamination of the secondary tapes, which corresponds to the failure of the interface between the system and the substrate, and in other cases by the breakage of the secondary tapes themselves. The occurrence of these two mechanisms suggests that the adhesive energy of the tape/substrate contact is high with respect to the fracture energy of the adhesive tapes, and that elastic deformation plays an important role in the total dissipated energy under load of the staple-pin system. The compliance of the adhesive tapes, associated with a low contact angle in such structures has been attributed to a spider strategy to develop maximum adhesive strength out of a minimum amount of material and artificial systems mimicking the spider attachment disc have recently been introduced [7], with the aim of optimizing the maximum detachment force and the total dissipated energy out of minimal contact area and material use.

Various theoretical approaches have been developed to treat thin film-peeling problems in the case of single [8] [9] and multiple tapes [10]. The objective of the latter is to describe the behaviour of a system containing various simultaneously detaching tapes [11], which apply to natural systems like gecko toes [12] as well as spider web anchorages. However, the behaviour under loading of multiple peeling systems is not trivial and ad hoc numerical procedures are required to simulate their delamination [13] [14]. Various numerical approaches have been developed to address specific problems, such as adhesion to various types of surfaces [15], influence of hierarchical structure [16], role of friction [17] and viscoelasticity [18]. These numerical modelling tools are

essential to design bioinspired artificial micro-patterned surfaces with optimized properties [19], including hierarchical structures [20].

Here, we develop analytical and numerical models to simulate the delamination and failure of coupled adhesive tapes, also taking into consideration the elastic deformation and the peeling angle variation under load of the staple-pin attachment. We propose a general numerical scheme to model the detachment of staple-pin-like structures, introducing new aspects to existing models such as tape fracture and 3-D deformation of the attachment devices. This work can help develop new designs for efficient bio-inspired attachments, maximizing adhesive strength while minimizing material use.

2. Model

We consider the geometry shown in Fig.1b. The attachment system is built from an array of tapes attached perpendicularly to the main cable on which a vertical external load is applied. Considering a single tape from the staple-pin structure, the problem reduces to studying the symmetric double peeling system shown in Fig. 1(c-d) [21]. As shown in the figure, for simplicity we consider the attached tape to be perfectly flat along its whole length, so that there is a discontinuity in its curvature at the location of the peeling line. This is an approximation whose validity decreases for increasing substrate softness or tape thickness.

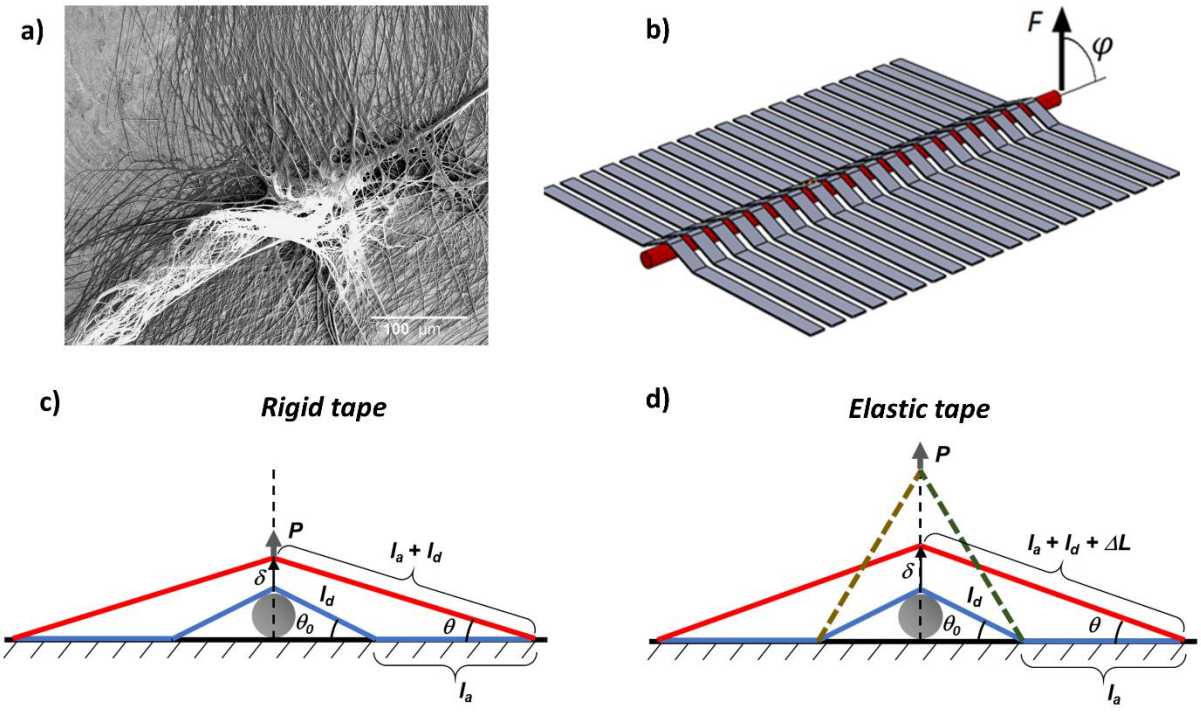

Figure 1: a) Spider web anchorage; b) Schematic representation of a staple-pin attachment structure: F is the applied external load, φ its angle with respect to the substrate. c)–d) The symmetric double peeling system viewed as a sub-domain of the staple-pin in the rigid (c) and elastic (d) tape cases. In d), the additional elastic deformation before delamination is illustrated with dashed lines. P is the applied load, l_a is the attached tape length, l_d is the detached tape length, ΔL is the tape elongation, δ is the vertical displacement of the load application point, θ_0 is the initial peeling angle, θ is the current peeling angle.

The detachment of tapes adhering to a substrate can be theoretically described using Griffith's energy balance. The energy release rate during delamination can be defined as the instantaneous variation of potential energy Π per unit area A, i.e. $G = -(d\Pi/dA)$. The peeling front advances when G reaches the critical energy release rate:

$$G = G_C \tag{1}$$

Writing the total potential energy as $\Pi = U_e - V$, where U_e is the stored strain energy and V the work associated with the external load acting on the system, this amounts to

$$\frac{1}{w}\left(\frac{\partial V}{\partial l_d} - \frac{\partial U_e}{\partial l_d}\right) = G_C \tag{2}$$

where l_d is the detached length of the tape and *w* its width.

2.1 Rigid tape case

We first consider an inextensible film, in which the contribution of the stored elastic energy is neglected ($U_e = 0$), which leads to the solution of the Rivlin equation [8]. According to the latter, delamination occurs when:

$$T(1 - \cos\theta) = wG_C \tag{3}$$

where *T* is the tape tension, θ is the peeling angle, i.e. the angle between the tape and the substrate. For the symmetric *V*-shaped double peeling system in Fig. 1b, the applied external load *P* is:

$$P = 2\sin\theta\, T \tag{4}$$

and peeling starts when the external load reaches the value P_{del}

$$P_{\mathrm{del}}(\theta) = \frac{2wG_C \sin\theta}{1 - \cos\theta} \tag{5}$$

Overall, from an initial tape-substrate angle configuration θ_0, when the external load is applied, the peeling angle decreases as the structure detaches. This behaviour is shown in a *P* vs. θ plot in Fig. 2, for *w* = 1 mm, $\theta_0 = 75°$ and three increasing G_C values: a) $G_C = 1$ kJ/m^2, b) $G_C = 2{,}5$ kJ/m^2, and c) $G_C = 4{,}5$ kJ/m^2. Starting from an unloaded structure ($P(\theta_0) = 0$, point O) and increasing *P*, the tapes will start to peel off at $P = P_{del}$ (point A), leading to a decrease in the peeling angle and consequently an increase in P_{del}. In this case, the peeling angle tends to zero as

the delamination proceeds and the peeling force increases indefinitely ($P_{\mathrm{del}} \to \infty$ for $\theta_0 \to 0$,). The admissible space of load-angle configurations is $\Omega = \{P \leq P_{\mathrm{del}}\}$.

We now introduce a critical tape tension T_c at which the tape fractures. Depending on the adhesive energy and the geometrical and mechanical properties of the system, three different behaviours can occur as a function of the critical energy release rate G_C (Fig. 2). When G_C is smaller than a given value G_1 ($G_C < G_1$, Fig. 2a), the tape delaminates over its full attached length l_a and the critical tension for fracture is not reached during the process. The limit angle before delamination can be derived from geometrical considerations (see Fig. 1c) as $\cos\theta_{lim} = (l_d \cos\theta_0 + l_a)/(l_a + l_d)$. Assuming now that the tape fractures immediately before reaching the peeling angle θ_{lim}, we derive from Eq.(3):

$$G_1 = \frac{T_c(1-\cos\theta_{lim})}{w} = \frac{T_c(1-\cos\theta_0)}{w}\frac{l_d}{l_a+l_d} \tag{6}$$

If G_C is greater than a second given value G_2 ($G_C > G_2$) the tape fractures before any delamination (and thus angle change) occurs. This happens when the external load reaches a critical value $P_c = 2\sin\theta T_C$ (Fig. 2c). Again, from Eq.(3) with $\theta = \theta_0$, we have:

$$G_2 = \frac{T_c(1-\cos\theta_0)}{w} = \frac{l_a + l_d}{l_d} G_1 \tag{7}$$

If G_C lies between G_1 and G_2, i.e. $G_1 < G_C < G_2$, the critical tension is reached after a finite delamination length (Fig. 2b).

The overall dissipated energy W depends on the energy release rate and the corresponding tape delamination behaviour, as well as the tape fracture energy:

$$W = \int_{l_d \sin\theta_0}^{l_d \sin\theta_0 + \delta} P \, d\eta + W_f \tag{8}$$

where δ is the displacement of the external load application point and $W_f = G_f bw$, where G_f is the critical energy release rate for tape fracture. For full delamination with no fracture occurring for $G_C < G_1$, the dissipated energy increases linearly with G_C up to the value:

$$W_{1-} = 2l_a wG_1 \tag{9}$$

If the critical energy release rate reaches the value $G_C = G_1$, the entire attached region peels off and the tape fractures at the final delamination point (tape fracture is assumed to take place instantaneously). This corresponds to the maximum of dissipated energy, since tape fracture energy should be additionally considered:

$$W_{1+} = 2l_a wG_1 + G_f bw \tag{10}$$

For G_C values between G_1 and G_2, the tape delaminates for part of its attached length and breaks when the applied load reaches P_c, with the dissipated energy W decreasing with delaminated tape length. From geometrical considerations (see Fig. 1c) and using Eq. (3), we can derive the delamination length l_C after which the tape breaks

$$l_C = l_d \left(1 - cos\theta_0 - \frac{wG_C}{T_C}\right)\frac{T_C}{wG_C} \tag{11}$$

Thus, the dissipated energy for $G_1 < G_C < G_2$ is:

$$W = 2l_C wG_C = 2l_d T_C \left(1 - cos\theta_0 - \frac{wG_C}{T_C}\right) + G_f bw \tag{12}$$

When $G_C > G_2$, the dissipated energy associated with the fracture of the tapes with no delamination is zero, and only fracture energy remains, i.e. $W_2 = G_f bw$. The three cases are illustrated in Fig. 2d, where the dissipated energy is plotted as a function of the critical energy release rate adopting the test parameters $l_d = l_a$ = 0,2 mm, T_c = 5 N and G_f = 10 kJ/m^2. The limit values G_1 and G_2 are both highlighted.

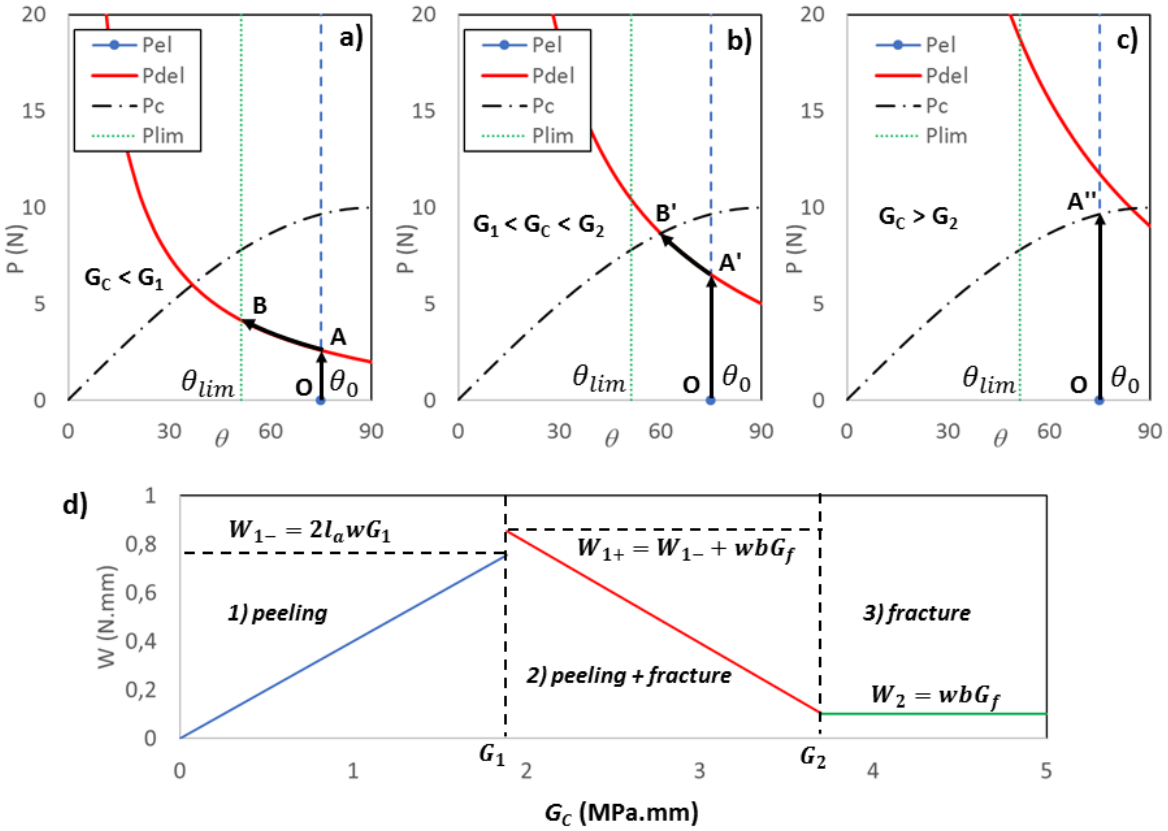

Figure 2: a)-c) External load P vs peeling angle θ for rigid tape symmetric double peeling for increasing critical energy release rate G_C. P_{el} is the initial load, P_{del} is the delamination load, Pc the critical (fracture) load. a) $G_C < G_{11}$: the tape delaminates over its entire attached length l_a until $\theta = \theta_{lim}$ (path OAB); b) $G_1 \leq G_C < G_2$: the tape delaminates and then fractures for P=P_c (path OA'B'); c) $G_C > G_2$: the tape fractures before delamination at $\theta = \theta_0$ (path OA''); d) Corresponding dissipated energy W vs. G.

2.2 Elastic tape case

Considering now additionally tape elastic deformation and its contribution to energy balance, Eq. (1) becomes the Kendall equation [9]:

$$T(1-\cos\theta)+\frac{T^2}{2Ewb}=wG_C \tag{13}$$

where b is the tape thickness and E is the tape elastic modulus. In this case, the peeling angle changes as a function of the elastic deformation and the detachment of the structure (Fig. 1d).

From a given initial configuration, it is possible to write the relationship between the tape strain ε and the tape-substrate angle θ when the tape deforms as:

$$l_d(1+\varepsilon)\cos\theta = l_d\cos\theta_0 \tag{14}$$

Writing the tape tension as $T = Ewb\varepsilon$, we obtain:

$$T = Ewb\left(\frac{\cos\theta_0}{\cos\theta}-1\right) \tag{15}$$

The external load $P = P_{el}$ for the initial elastic deformation of the structure shown in Fig.1d is therefore:

$$P_{el}(\theta) = 2\sin\theta\, T = 2\sin\theta Ewb\left(\frac{\cos\theta_0}{\cos\theta}-1\right) \tag{16}$$

which for any given θ assumes its maximal value for an initial peeling angle of $\theta_0 = 0$.

As discussed in previous works ([10], [14] [21]), the overall delamination problem can be treated as the superposition of two independent single peeling processes, with each tape loaded by its peeling tension. The external load at delamination P_{del} for a given critical energy release rate G_C is:

$$P_{del}(\theta) = 2\sin\theta Ewb\left(\cos\theta-1+\sqrt{(1-\cos\theta)^2+\frac{2G_C}{Eb}}\right) \tag{17}$$

When $P \geq P_{\text{del}}$, delamination occurs. As discussed in [14], Eq. (15) is valid only for peeling angles θ greater than the curve maximum occurring at $\theta = \theta_{\max}$, which corresponds to an initial loading angle of $\theta_0 = 0$, since smaller θ angles correspond to negative initial loading angles. From these considerations, we obtain the admissible space of load-angle configurations as $\Omega = \{P(\theta) \leq P_{\text{del}}(\theta) \cap P(\theta) \leq P_{\text{el}}(\theta)\}$.

The behaviour is shown in Fig.3 a), b), c), for test parameters w =1 mm, b = 0.01mm, E = 1 GPa, l_{d} =0,22 mm, l_{a} =1 mm, $\theta_0 = 75°$, $G_f = 5$ kJ/m^2 and three increasing G_C values: a) $G_C = 1{,}8$ kJ/m^2, b) $G_C = 3$ kJ/m^2, and c) $G_C = 5$ kJ/m^2. If the critical energy release rate is below G_1, for a given unloaded structure ($P(\theta_0) = 0$, point O), the system will first undergo elastic deformation without delamination (segment OA, along $P = P_{el}$), and then both elastic deformation and delamination with a variable peeling angle (segment AB). The tape will then fully detach when its entire finite length delaminates at $\theta = \theta_{lim}$ (point B). Alternatively, if l_a is sufficient for θ_{lim} to reach θ_{max}, the system will attain an equilibrium state where delamination proceeds at a constant peeling angle and load [14]. The corresponding peeling angle θ_{max} can be derived by equating Eq. (14) for $\theta_0 = 0$ and Eq. (15), leading to:

$$2\cos^3\ \theta_{max} - \left(3 + \frac{2G_C}{Eb}\right)\cos^2\theta_{max} + 1 = 0 \tag{18}$$

whose (real) root can be obtained in closed form as:

$$\cos\ \theta_{max} = \frac{(\beta - \alpha)[(1 - i\sqrt{3})\alpha - (1 + i\sqrt{3})\beta]}{12\beta} \tag{19}$$

with $\alpha = \left(3 + \frac{2G_C}{Eb}\right)$ and $\beta = \sqrt[3]{[\alpha^3 + 6(\sqrt{81 - 3\alpha^3} - 9)]}$. In the case $\theta_0 = 0$, this equilibrium state would be reached as soon as the first delamination occurs. The more general case of $\theta_{lim} < \theta_{max}$ is considered in Fig. 3a. Introducing, as for the rigid tape case, a fracture threshold T_C, for

$G_C = G_1$, the tape fractures when it reaches θ_{lim}. From geometrical considerations (see Fig. 1c), since the tape elongation at fracture is $\Delta L = T(l_a + l_d)/Ewb$, we obtain

$$\cos\theta_{lim} = \frac{l_a + l_d cos\theta_0}{l_a + l_d} \Big/ \left(1 + \frac{T_C}{Ewb}\right) \tag{20}$$

which gives the correct θ_{lim} value for the rigid tape case if $E \to \infty$.

When $G_C = G_1$, T_C can be written as:

$$T_C = Ewb\left(\cos\theta_{lim} - 1 + \sqrt{(1-\cos\theta_{lim})^2 + \frac{2G_1}{Eb}}\right) \tag{21}$$

so that

$$G_1 = (1-\cos\theta_{lim})\frac{T_C}{w} + \frac{T_C^2}{2Ew^2b} \tag{22}$$

which again gives the correct value provided in Eq. (6) for the rigid tape case ($E \to \infty$). Notice that if $\theta = \theta_{max}$ occurs for $G_C < G_1$, no tape fracture occurs, since delamination proceeds thereupon at a constant load.

For an increasing critical energy release rate ($G_1 \leq G_C < G_2$), the tape deforms (segment OA'), then delaminates, and fractures in B' as the limit angle is reached (Fig. 3b). Finally, for $G_C > G_2$the tape deforms elastically and fractures in A'' before delamination starts (Fig. 3b). The value of G_2 can be obtained from Eq. (11) for $\theta = \theta_0$ combined with Eq. (13), giving:

$$G_2 = \left(1 - \frac{\cos\theta_0}{(T_C/Ewb + 1)}\right)\frac{T_C}{w} + \frac{T_C^2}{2Ew^2b} \tag{23}$$

which is thus dependent on θ_0. This expression tends to that in Eq. (7) for $E \to \infty$.

The dissipated energy W in the elastic tape case is the sum of the released adhesive, elastic and fracture energies:

$$W = U_{el} + U_{del} + W_f = \int_{l_d \sin\theta_0}^{l_d \sin\theta_0 + \delta} P \, d\eta + wbG_{\mathrm{f}} \tag{24}$$

where U_{el} is the elastic energy stored in the deformed tape when complete detachment or fracture occurs. Thus, for $G_C < G_1$, W increases linearly with G_C as:

$$W = 2(l_a + l_d)\frac{{T_C}^2}{2Ewb} + 2l_a wG_C \tag{25}$$

reaching a maximum value $W_{1+} = W_{1-} + wbG_{\mathrm{f}}$ in G_1, where the additional tape fracture energy leads to a discontinuity in W. After this maximum value, W decreases with G as the delamination length decreases:

$$W = 2(l + l_d)\frac{{T_C}^2}{2Ewb} + 2lwG_1 + wbG_{\mathrm{f}} \tag{26}$$

where $l = l(G_C, \theta_0)$ is the delamination length before tape fracture, which is also dependent on the initial angle θ_0. Finally, the dissipated energy for $G_C > G_2$ is constant and only due to the elastic deformation and fracture terms:

$$W_2 = 2l_d \frac{{T_c}^2}{2Ewb} + wbG_{\mathrm{f}} \tag{27}$$

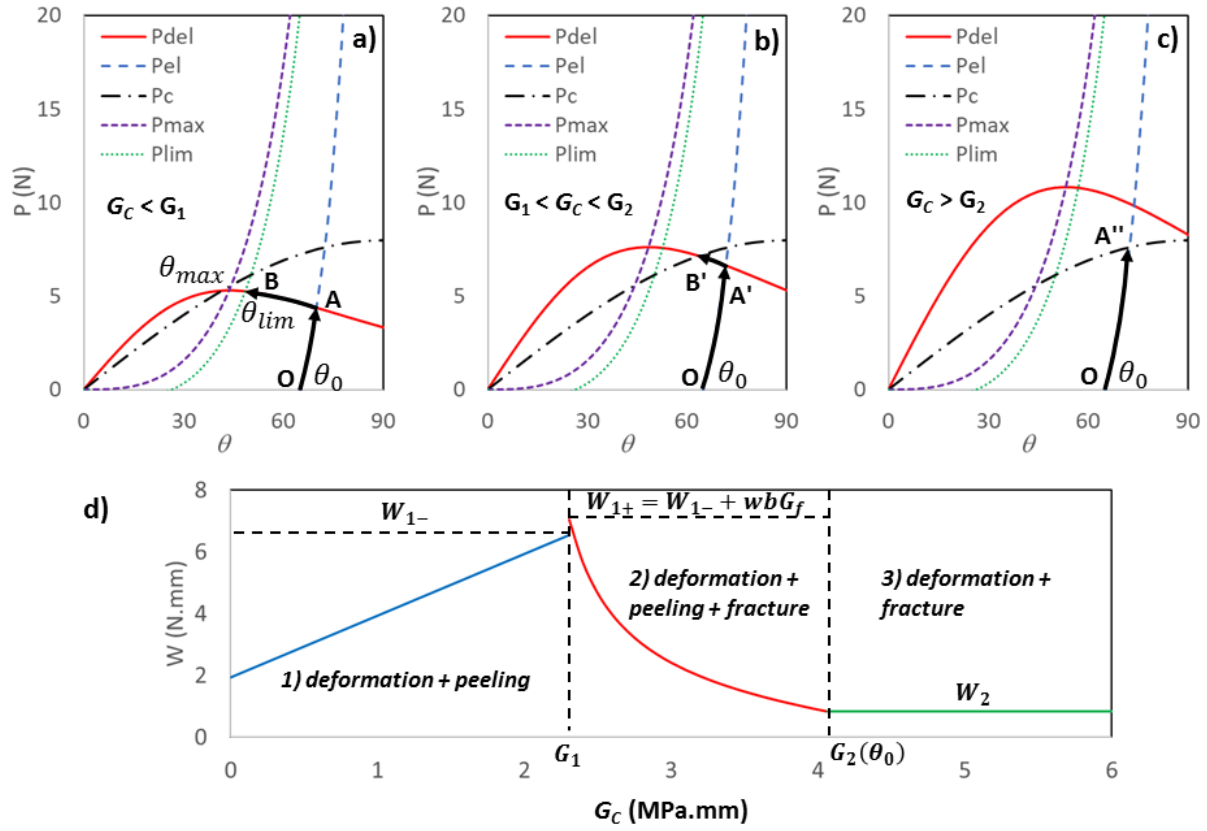

Figure 3: a)-c) External load P vs peeling angle θ for elastic tape symmetric double peeling for increasing critical energy release rate G_C. P_{el} is the load for elastic deformation, P_{del} is the delamination load, Pc the critical (fracture) load, P_{max} the maximum peeling load, P_{lim} the load for complete delamination of the attached tape length l_a. a) $G_C < G_1$: the tape deforms (path OA) and then delaminates (path AB) over l_a until $\theta = \theta_{lim}$; b) $G_1 \leq G_C < G_2$: the tape deforms (path OA'), delaminates (path A'B') and then fractures for P=P_c; c) $G_C > G_2$: the tape deforms (path OA'') and fractures before delamination for P=P_c; d) Corresponding dissipated energy W vs. G_C.

The load vs. displacement curve in the optimal case $G_C = G_1$ is shown in Figure 4, together with the contribution of the elastic and delamination energy. The resulting curve displays a perfect elastoplastic behaviour.

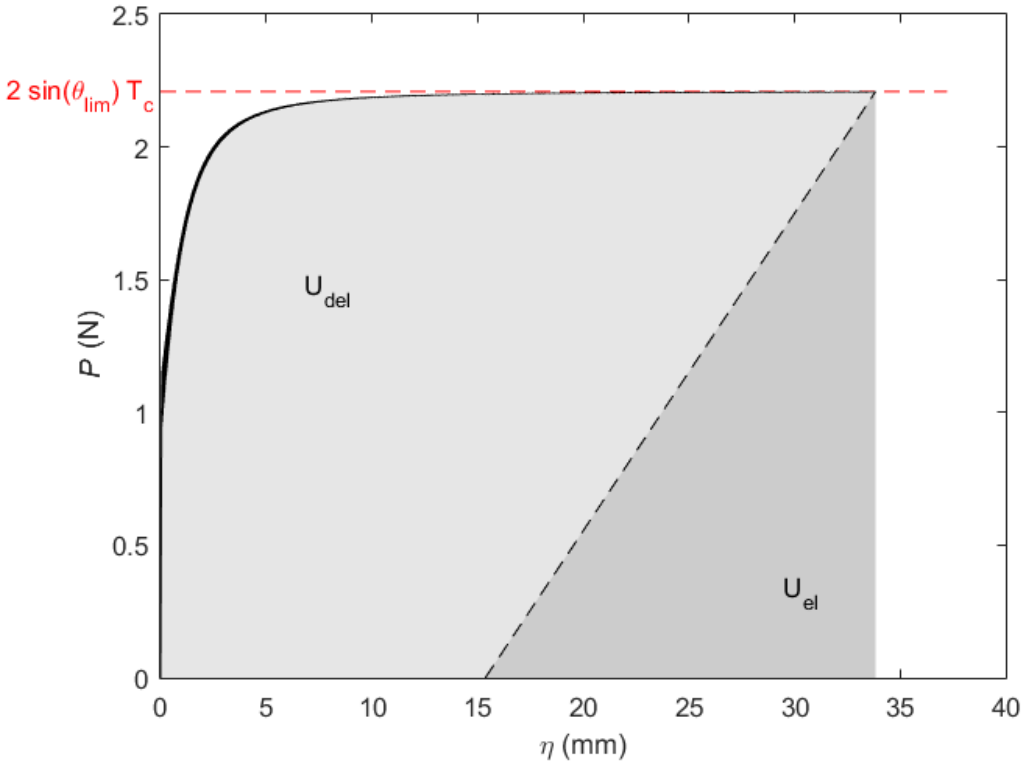

Figure 4: External load as a function of the displacement at the load application point during the detachment of a symmetric double peeling elastic tape when the adhesive energy is optimal. The energy dissipated during detachment and the stored elastic energy are shown as shaded areas.

Notice that the above discussion can be generalized from a 2D to 3D structure, in which the deformed detached length of the tape is not aligned with the delamination direction, as illustrated in Figure 5. In this case, Eq. (3) is modified as follows:

$$T(1 - \cos\theta \cos\lambda) = wG \tag{28}$$

where λ is the angle defining the misalignment of the detached tape and attached length, due to deformation or initial conditions. Since the elastic energy variation and the surface energy remain unchanged, Eq. (13) becomes:

$$T(1-\cos\theta\cos\lambda)+\frac{T^2}{2Ewb}=wG \tag{29}$$

When both attached and detached tape are aligned ($\lambda=0$) the above equation coincides with Eq. (13). Solving Eq. (29) provides the tension needed to detach the tape:

$$T_1=2Ewb\left(\cos\theta\cos\lambda-1+\sqrt{(1-\cos\theta\cos\lambda)^2+\frac{2G}{Eb}}\right) \tag{30}$$

These equations are valid under the hypothesis that even when $\lambda\neq 0$, the load is equally distributed over the peeling line, and that the width of the peeling line remains unchanged (with respect to $\lambda=0$). This could be an over-simplification of the problem in some cases, and local load concentrations could appear, with a reduction of the peeling force.

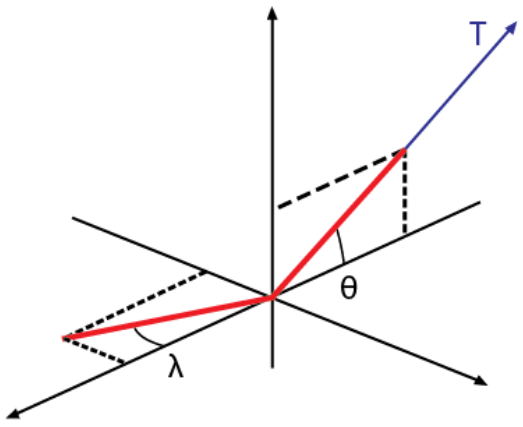

Figure 5: Misalignment between the attached and detached tape.

3. Numerical implementation

To simulate the delamination and fracture behaviour of arbitrary multiple tape structures, we adopt a general numerical model based on mechanical equilibrium and energy balance. For a given structure in 3-D space, mechanical equilibrium is obtained using the co-rotational truss formulation [22].

The system is built using a frame of truss members sustaining axial load only, where the elements in contact with the substrate act as peeling tapes. The bending stiffness is therefore neglected. A member k of the system linking the nodes i and j, is defined by its initial length l, thickness b, width w, elastic modulus E. The stiffness k_k of the k-th truss member in the local coordinate system (1D along the axis of the truss member) is:

$$k_k = E_k b_k w_k / l_k \tag{31}$$

The material stiffness of this element in the global coordinate system (3D) is obtained constructing the transformation vector:

$$\mathbf{L} = [c_1 \quad c_2 \quad c_3 \quad -c_1 \quad -c_2 \quad -c_3] \tag{32}$$

where c_1, c_2 and c_3 are the element direction cosines in 3-D space:

$$c_1 = \frac{x_j - x_i}{l_k} \tag{33}$$

$$c_2 = \frac{y_j - y_i}{l_k} \tag{34}$$

$$c_3 = \frac{z_j - z_i}{l_k} \tag{35}$$

and $\mathbf{x} = [x \quad y \quad z]$ is the coordinate vector of a node under deformation of the system. The material stiffness matrix $\mathbf{K_m}$is then written as

$$\mathbf{K_m} = k_k \, \mathbf{L}^{\mathrm{T}} \mathbf{L} \tag{36}$$

The external force vector $\mathbf{Q_e}$ contains the components of the external load acting on the system. Rather than directly solving the linear system in terms of nodal displacements $\mathbf{K_m u} = \mathbf{Q_e}$, iterative scheme is implemented to address the geometrical nonlinearity arising from this type of mechanical system. Indeed, large rotations of the truss members are expected, which need to be taken into account in order to obtain an accurate displacement field. We introduce the geometric stiffness matrix as

$$\mathbf{K_g} = \frac{k_k \delta l_k}{l_k + \delta l_k} \mathbf{H} \tag{37}$$

where δl_k is the elongation of the deformed element, $\mathbf{H} = \mathbf{h}^{\mathrm{T}}\mathbf{h}$, and $\mathbf{h} = [-\mathbf{I} \quad \mathbf{I}]$. The truss member contribution to the internal force vector is:

$$\mathbf{Q_i} = k_k \delta l_k \, \mathbf{L}^{\mathrm{T}} \tag{38}$$

Once all contributions are assembled in the linear system, mechanical equilibrium is obtained by updating the nodal displacement according to the following iterative scheme:

$$\mathbf{u} + \left(\mathbf{K_m} + \mathbf{K_g}\right)^{-1} (\mathbf{Q_e} - \mathbf{Q_i}) \rightarrow \mathbf{u} \tag{39}$$

The 2-norm of the residual $\|\mathbf{Q_e} - \mathbf{Q_i}\|$ is used as convergence criterion. Therefore, the equilibrium between internal and external loads is verified, including in the case of large rotations.

In order to control the tape delaminations, the external load is incremented iteratively, and the total potential energy variation is calculated at each increment. The delamination of a discrete length Δl of a member in contact with the substrate leads to a modification of its length (and therefore its stiffness) and of the coordinates of the node in contact:

$$l + \Delta l \rightarrow l \tag{40}$$

$$\mathbf{x} + \Delta\mathbf{x} \rightarrow \mathbf{x} \tag{41}$$

The change in the attached node coordinate depends on the direction of the attached part of the delaminating tape respect to the detached one. It has two components on the x-y substrate plane and a zero value in the z direction ($\Delta l = \sqrt{\Delta x + \Delta y}$). At each step of the simulation, the energy variation is verified for all the members in contact, between the current state (a) and the state where the considered tape detachment has been incremented (b). The work variation associated with the detachment of the tape *k* is the 1-norm of the product of the external force vector and the difference between displacement after and before detachment.

$$\frac{\Delta V}{\Delta l} = |\mathbf{Q_{ext}}(\mathbf{u_b} - \mathbf{u_a})| \tag{42}$$

The variation of elastic energy in the system is obtained as:

$$\frac{\Delta U_e}{\Delta l} = \frac{1}{2}\sum_{k=1}^{N}\left[\left(k_k \delta {l_k}^2\right)_b - \left(k_k \delta {l_k}^2\right)_a\right] \tag{43}$$

where *N* is the total number of truss members in the system. Detachment occurs when:

$$\frac{\Delta V}{\Delta l} - \frac{\Delta U_e}{\Delta l} > wG_C \tag{44}$$

Figure 6 illustrates the method used to check whether a tape has delaminated or not for a simple V-shaped tape system observed in the x-z plane. The displacement field of the system as a response to the external load is first computed (Figure 6a). Then, for each element in contact with the substrate, the detached length of the element is incremented and the tape length and its attached node coordinates updated. The new displacement field is then computed to test if the element has delaminated, as shown in Figure 6b for the first element delamination test. We then check if detachment has occurred by calculating the variation of potential energy in (44). If not, the system

is reset and the next element delamination is verified. If no delamination is observed, the external load is incremented, and so on until the whole system has been fully detached.

Tape fracture is introduced by a simple removal rule when one of the tape tensions reaches the critical value T_c. If the tape geometry and loading are in the same plane, the system can be reduced to a 2-D problem.

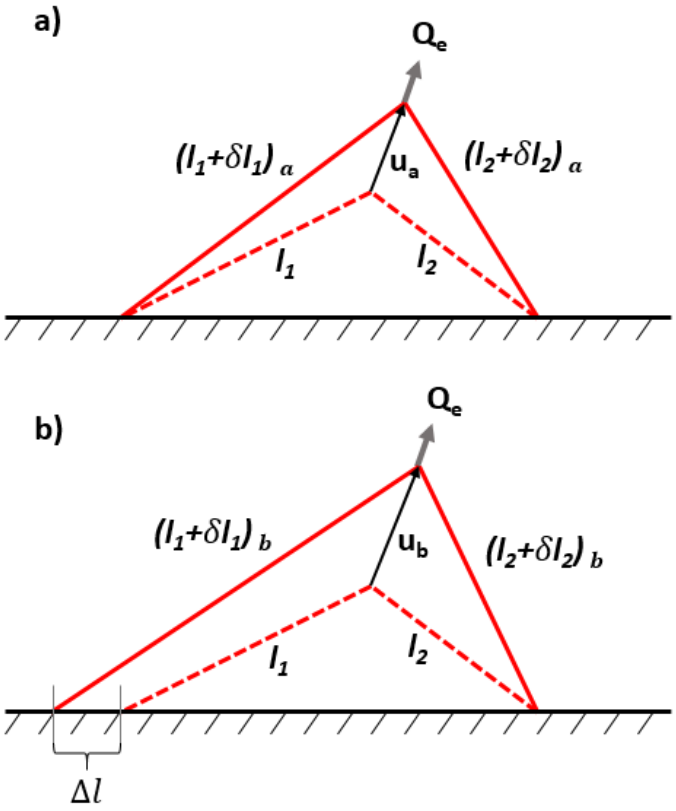

Figure 6: a) Current deformed state (state a) of a V-shape 2D attachment system under load. b) Increment in the first tape detached length.

4. Numerical results

We use the previously described numerical method to model the complete staple-pin system shown in Figure 1. The dragline, or cable that supports the external load is assumed to have a diameter $d^* = 0.2$ mm with a circular cross section $A^* = \pi {d^*}^2$, an elastic modulus $E^* = 100$ MPa and a length $L^* = 100$ mm, for a total number of $N^* = 50$ transversal tapes. We assume for each of these tapes the following properties: $w = 1$ mm, $b = 0.01$ mm, $E = 100$ MPa, $l_a = 50$ mm, $\theta_0 = \pi/16$, $l_d = d^*/\sin\theta_0$ and $T_C = 0.2$ N. An example of the global load response, together with the evolution of the deformed and peeled system is shown in Figure 7.

We first consider the case in which the critical energy release rate G_C is small enough for the system to completely peel-off over its entire attached regions without any fracture ($G_C = 0.04$ kJ/m^2), applying a load perpendicular to the substrate at $\theta = \pi/2$. The corresponding overall load-displacement curve is shown in Figure 7a, displaying an initial quasi-linear behaviour, and then a constant-load plastic branch, where an equilibrium is reached as the secondary transversal tapes are delaminating. The whole structure detaches at approximately constant load, apart from small oscillations in the force value due to the delaminating tapes. Various snapshots of the deformation profile of the entire structure as it delaminates are shown in Figure 7b, highlighting the advancing delamination front as the load application point displacement increases. The overall adhesive force F as a function of the critical energy release rate is shown in Figure 7c, again for an external load perpendicular to the substrate $\varphi = \pi/2$. This highlights the discussed transition from delamination to fracture behaviour of the tapes at $G_1 = 0.05$ kJ/m^2. This value coincides with the optimal critical energy release rate predicted with Eq. (19).

To analytically predict the global peeling force, energy balance expressed in Eq. (2) can be applied to the cable. The interaction between the cable and the substrate occurs through the transversal tapes, each of which can dissipate a total amount of energy W given by Eq. (24). Dividing this

value by the width of the tapes gives the energy per unit length needed to detach the cable. Using Eq. (13), the energy balance applied directly to the cable becomes:

$$F(1-\cos\theta)+\frac{F^2}{2E^*A^*}=\frac{W}{w} \tag{45}$$

Thus, the global peeling force becomes:

$$F=2E^*A^*\left(\cos\theta-1+\sqrt{(1-\cos\theta)^2+\frac{2W}{wE^*A^*}}\right) \tag{46}$$

Comparing the maximum peeling force obtained in the simulations with the theoretical one (indicated as F_1) in Eq.(20), Eq. (25) and Eq. (46), a good agreement is found (Figure 7c).

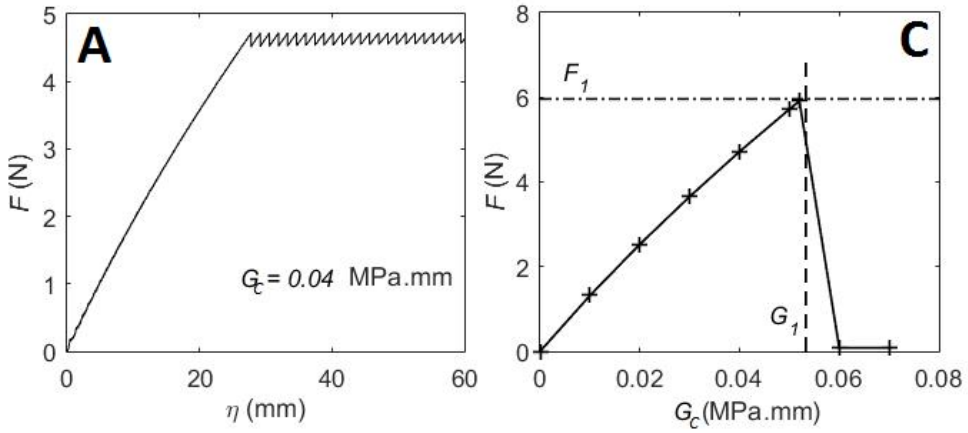
A
F (N)
η (mm)
G_c = 0.04 MPa.mm
C
F_1
G_1
F (N)
G_c (MPa.mm)

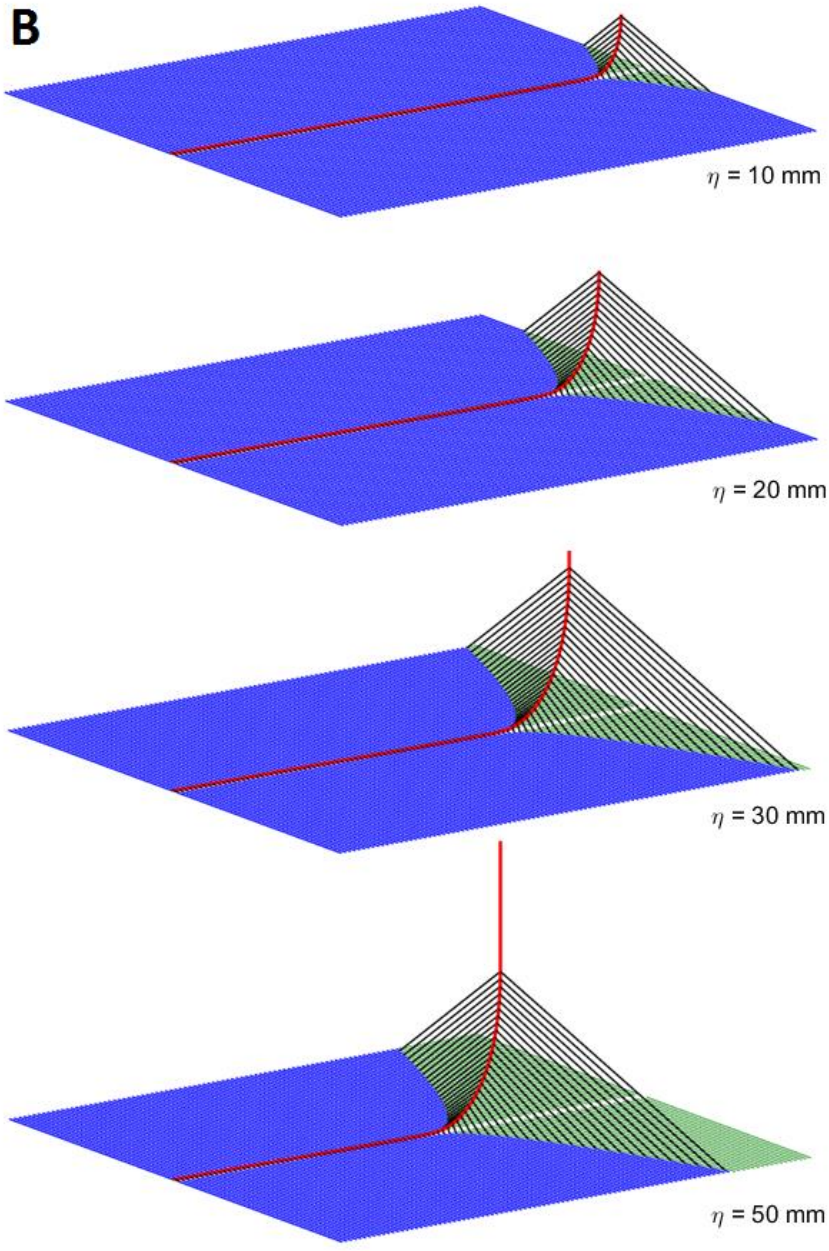
B
η = 10 mm
η = 20 mm
η = 30 mm
η = 50 mm

Figure 7: a) External load to displacement of the load application point during detachment of the staple-pin structure obtained from the numerical model. b) Corresponding evolution of the system (the red line is the cable, the black lines are the detached tape regions, the blue lines are the attached tape regions and the green line are the detachment path of the adhesive tapes. The fully detached tapes are not represented). C. Overall detachment force as a function of the adhesive energy obtained from the numerical model, plotted together with the theoretical optimum.

5. Experimental validation

To further verify the validity of the presented model, a comparison is made with experimental results from [7], where artificial staple-pin attachment discs were fabricated through electrospinning and tested in peeling experiments on aluminium substrates with variable adhesive characteristics. As schematically shown in Fig. 8a, a 30μm-diameter nylon fibre was pulled at a peeling angle of $\theta = \pi$, leading to the delamination, deformation and fracture of perpendicularly placed polyurethane fibres. Typically, this lead to a delamination zone of relatively constant width, as shown in Fig. 8b. Having derived single fibre tensile properties up to fracture, it was therefore possible to estimate for each tested attachment disc the dissipated energy in peeling and in deformation up to fracture, as described in [7]. The larger the delaminated width, the larger the dissipated energy. Three different substrate adhesive properties were considered, i.e. a perfluoro-plasma treated aluminium substrate, an untreated substrate, and an oxygen-plasma treated aluminium substrate (in order of increasing adhesive properties). This allows us to compare model predictions to experimentally measured points.

A single polyurethane fibre in the staple-pin structure has a diameter of 1.5 μm and an initial detached length approximately equal to the radius of the nylon fibre: l_d = 15.0 μm. Its Young's modulus E and critical tension T_C are derived from tensile tests as E= 10.7 MPa and T_C = 39.9 μN. The spacing between fibres is approximately s = 15 μm. The average delaminated lengths before fracture for the three considered substrates are l_1 = 2.01 mm, l_2 = 1.71 mm, l_3 = 0.45 mm. Since in all three cases fracture takes place after the transversal fibres have partially delaminated, the experimental scenario corresponds to the case $G_1 < G_C < G_2$. The G_C values of the three experimental points are determined from their delaminated length values l_i using Eq. (20) and Eq. (13). The total dissipated energy per unit length (of the nylon fibre) can be derived by taking the integral of the experimental force/displacement curves and dividing them by L_0, and corresponds in the three cases to W_{T1}/L_0 = 0.065 J/m, W_{T2}/L_0 = 0.050 J/m, W_{T3}/L_0= 0.029 J/m. The contribution of energy (per unit L_0) due to stretching of the fibres can be estimated from the integral of the single fibre tensile loading curves, multiplied by the number of fibres n, as

$$W_S/L_0 = 2\left(\int \sigma d\varepsilon\right)\pi\left(\frac{d}{2}\right)^2 l\frac{n}{L_0} = \left(\int \sigma d\varepsilon\right)\frac{\pi d^2 l}{2s} \tag{47}$$

and corresponds in the three cases to $W_{S1}/L_0 = 3.1\cdot10^{-3}$ J/m, $W_{S2}/L_0 = 2.2\cdot10^{-3}$J/m, $W_{S3}/L_0 = 2.6\cdot10^{-3}$ J/m. Here, the entire fibre diameter is used to estimate the contact width of the fibres.

These experimental values can be compared to theoretical values, using the system geometrical and mechanical parameters: first, $cos\theta_{lim}$ is calculated from Eq. (20), and from it, G_1 and G_2 using Eq. (22) and Eq. (23). Then, the corresponding dissipated energy W_T is derived using Eq. (26) and multiplying it by the number of fibres, after having determined $G_C = G_C(l, \theta_0)$ from Eq. (20).

Results are shown in Fig. 8c, in terms of dissipated energy (per unit disc length L_0) as a function of critical energy release rate, having assumed for simplicity $\theta_0 \sim 90°$. The experimental data are compatible with the model predictions, i.e. the total energy dissipated during peeling is found to be higher for surfaces with smaller work of adhesion [7]. This results in larger volume of threads getting deformed during peeling, and in higher total energy dissipated during the peeling process.

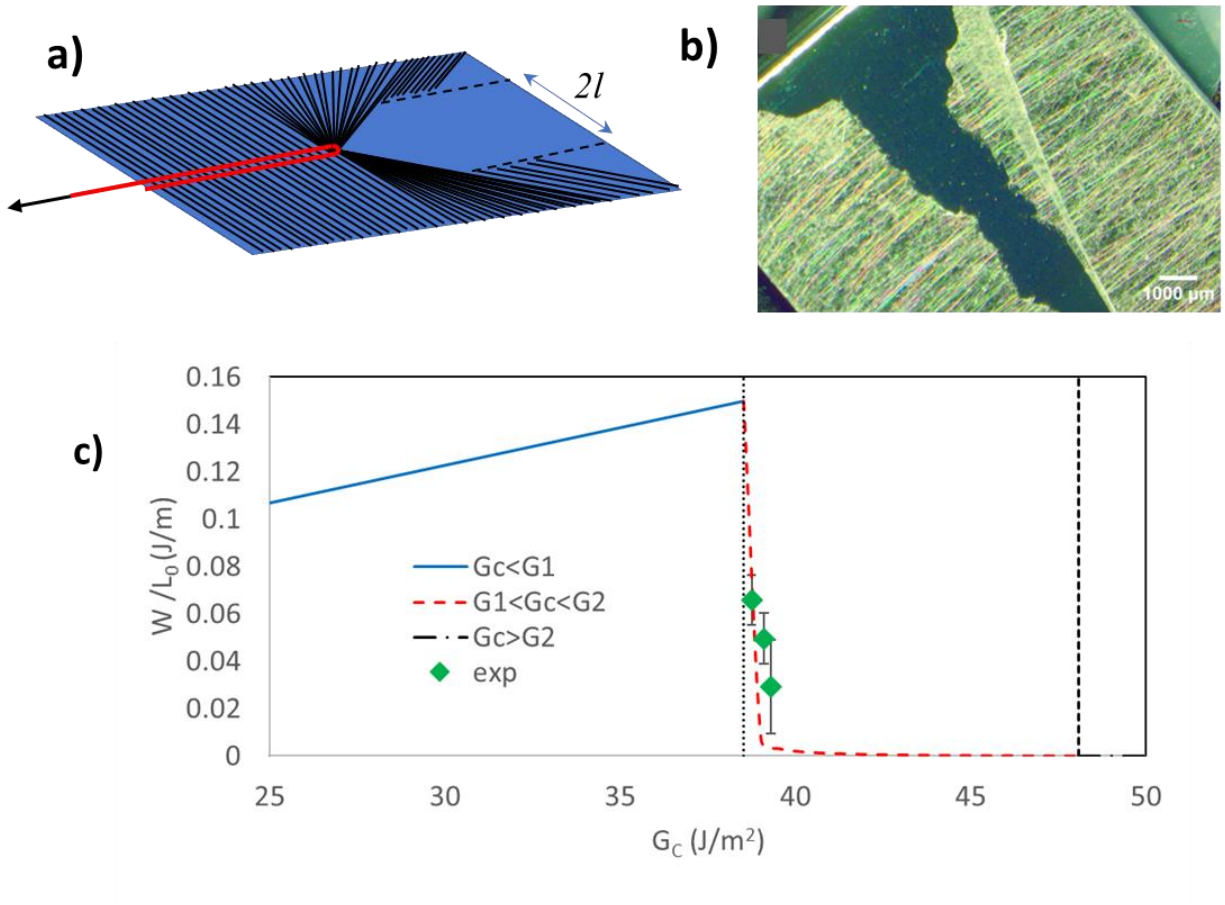

Figure 8: a) Schematic of experimental test, with staple pin architecture pulled at $\theta = \pi$; b) optical image of the peeling behaviour of a disc prepared on an oxygen plasma treated substrate: the peeling starts with a w-shaped zone but proceeds with delamination over a relatively uniform width; c) comparison between model predictions and experimental data for dissipated energy per unit disc length L_0 as a function of the critical energy release rate.

6. Discussion

Numerical and experimental data confirm model predictions that the global adhesive force of the system is obtained from the energy dissipated by discrete sub-regions rather than from the maximum force they can carry. This has non-trivial consequences. Spiders employ multiple types of silks with different modulus and architecture to maximize the total work during attachment, rather than maximizing the maximum detachment force. For example, viscid silk threads used for capturing flying or walking preys uses stretch flagilliform silk threads coated with glue droplets [4] [23]. During peeling the glue droplets stretch and results in the formation of a suspension bridge-like structure, with the force distributed over a much larger volume of the silk thread [24]. This again results in maximizing the total energy dissipated during peeling as a result of stretching the flagilliform thread and multiple glue droplets, in addition to the thermodynamic work of adhesion.

In the case of pyriform attachment disks, recent work has highlighted how these structures are particularly efficient in providing high pull-off resistance, as well as robust, given the large variation in the pulling angles occurring in a real environment [5]. Also, it has been shown that silk anchor structure evolved and was optimized over millions of years, with considerable effects on the robustness of web attachment [25]. The large adhesion energy of the attachments prevents the threads from peeling and this results in less energy spent in stretching the peeled threads. Therefore, the total energy involved in peeling is reduced.

Additionally, in biological adhesion, typical structures often display a hierarchical architecture, which means that energy dissipation mechanisms occur at different scale levels simultaneously, each of them having a specific response to different load distributions over its sub-units. At present,

most of the studies are focused on the detachment force of the contact units [26]. The present work shows that from a lower to an upper level, the dissipated energy of each contact is more important than its maximum detachment force. This is particularly important in cases in biological adhesion where most of the contacts are realized using tape-like units, displaying a typical “elastoplastic” behaviour such as that shown in Figure 4, where the maximum detachment force is not sufficient to determine the total dissipated energy.

Conclusions

We have studied fibrous or tape-like attachment systems with multiple contacts, such as those found in staple-pin structures in spider webs, introducing a general analytical scheme that includes both delamination and tape fracture, and validating it with numerical simulations. We have shown that adhesive energy and mechanical strength are synergetic in providing optimized load-bearing properties, i.e. the maximum load an attachment can support before detachment. Additionally, we have shown that the energy dissipated by the contacts, accounting both for elastic deformation and detachment, determines the adhesive force of a multiple peeling system.

Since structures formed by arrays of contact units, usually tape-like contacts, are recurrent in biological adhesives, the model discussed could help to improve the understanding of Nature’s strategies to enhance and optimize adhesion. This approach could also be useful in future for the design and optimization of artificial bioinspired adhesives.

Acknowledgements

F.B. is supported by H2020 FET Proactive "Neurofibres" grant No. 732344, by the project “Metapp” (n. CSTO160004) funded by Fondazione San Paolo, and by the Italian Ministry of

Education, University and Research (MIUR), under the “"Departments of Excellence”" grant L. 232/2016. NMP is supported by the European Commission under the Graphene Flagship Core 2 Grant no. 785219 (WP14 “Composites”) and FET Proactive “Neurofibres” Grant no. 732344 as well as by the Italian Ministry of Education, University and Research (MIUR) under the “Departments of Excellence” Grant L.232/2016, the ARS01-01384-PROSCAN Grant and the PRIN-20177TTP3S. This work was carried out within the COST Action CA15216 “European Network of Bioadhesion Expertise: Fundamental Knowledge to Inspire Advanced Bonding Technologies”. Computational resources were provided by the C3S centre at the University of Torino (c3s.unito.it) and by hpc@polito (www.hpc.polito.it).

References

[1] Nova, A., Keten, S., Pugno, N. M., Redaelli, A., & Buehler, M. J., "Molecular and nanostructural mechanisms of deformation, strength and toughness of spider silk fibrils.," *Nano letters,* vol. 10, no. 7, pp. 2626-2634, 2010.

[2] Cranford, S. W., Tarakanova, A., Pugno, N. M., & Buehler, M. J., "Nonlinear material behaviour of spider silk yields robust webs.," *Nature,* vol. 482, no. 7383, pp. 72-76, 2012.

[3] Wolff, J. O., Grawe, I., Wirth, M., Karstedt, A., & Gorb, S. N., "Spider's super-glue: thread anchors are composite adhesives with synergistic hierarchical organization.," *Soft Matter,* vol. 11, no. 12, pp. 2394-2403, 2015.

[4] Sahni, V., Harris, J., Blackledge, T. A., & Dhinojwala, A., "Cobweb-weaving spiders produce different attachment discs for locomotion and prey capture.," *Nature communications,* vol. 3, 2016.

[5] J. O. Wolff and M. Herberstein, "Three-dimensional printing spiders: back-and-forth glue application yields silk anchorages with high pull-off resistance under varying loading situations," *J. R. Soc. Interface,* vol. 14 , p. 20160783, 2017 .

[6] Grawe, Ingo, Jonas O. Wolff, and Stanislav N. Gorb., "Composition and substrate-dependent strength of the silken attachment discs in spiders.," *Journal of The Royal Society Interface,* vol. 11, no. 98, 2014.

[7] Jain, Dharamdeep, Vasav Sahni, and Ali Dhinojwala., "Synthetic adhesive attachment discs inspired by spider's pyriform silk architecture.," *Polymer Science Part B: Polymer Physics,* vol. 52, no. 8, pp. 553-560, 2014.

[8] R. S. Rivlin, "The effective work of adhesion.," *Collected Papers of RS Rivlin. Springer New York,* pp. 2611-2614, 1997.

[9] K. Kendall, "Thin-film peeling-the elastic term," *Journal of Physics D: Applied Physics,* vol. 8, no. 13, p. 1449, 1975.

[10] N. M. Pugno, "The theory of multiple peeling," *International journal of fracture,* vol. 171, no. 2, pp. 185-193, 2011.

[11] F. Bosia, S. Colella, V. Mattoli, B. Mazzolai and N. M. Pugno, "Hierarchical multiple peeling simulations," *RSC Advances,* vol. 4, no. 48, pp. 25447-25452, 2014.

[12] H. Yao and H. Gao, "Mechanics of robust and releasable adhesion in biology: Bottom–up designed hierarchical structures of gecko," *Journal of the Mechanics and Physics of Solids,* vol. 54, no. 6, pp. 1120-1146, 2006.

[13] İ. Özdemir, “A numerical solution framework for simultaneous peeling of thin elastic strips from a rigid substrate.,” *Acta Mechanica,* pp. 1-13, 2017.

[14] L. Brely, F. Bosia and N. Pugno, “Numerical implementation of multiple peeling theory and its application to spider web anchorages,” *Interface Focus,* vol. 5 , p. 20140051, 2015 .

[15] L. Brely, F. Bosia and N. and Pugno, “The influence of substrate roughness, patterning, curvature and compliance in peeling problems,” *Bioinspiration & Biomimetics,* vol. 13 , p. 026004, 2017.

[16] L. Brely, F. Bosia and N. Pugno, “Emergence of the interplay between hierarchy and contact splitting in biological adhesion highlighted through a hierarchical shear lag model,” *Soft Matter,* vol. 14, pp. 5509-5518 , 2018.

[17] O. M. Braun, I. Barel and M. Urbakh, “Dynamics of transition from static to kinetic friction,” *Physical Review Letters,* vol. 103, no. 19, p. 194301, 2009.

[18] B. Lorenz, B. Krick, N. Mulakaluri, M. Smolyakova, S. Dieluweit, W. Sawyer and P. BNJ, “Adhesion: role of bulk viscoelasticity and surface roughness,” *J. Phys.: Condens. Matter,* vol. 25, p. 225004, 2013.

[19] M. T. Northen, C. Greiner, E. Arzt and K. L. Turner, “A Gecko-Inspired Reversible Adhesive,” *Advanced Materials,* vol. 20, p. 3905–3909, 2008.

[20] D. Brodoceanu, C. .. Bauer, E. Kroner, E. Arzt and T. Kraus, “Hierarchical bioinspired adhesive surfaces—a review,” *Bioinspiration & Biomimetics,* vol. 11, no. 5, 2016.

[21] Afferrante, L., Carbone, G., Demelio, G., & Pugno, N., “Adhesion of elastic thin films: double peeling of tapes versus axisymmetric peeling of membranes.,” *Tribology Letters,* vol. 52, no. 3, pp. 439-447, 2013.

[22] M. A. Crisfield and G. F. Moita, “A co-rotational formulation for 2-D continua including incompatible modes,” *International Journal for Numerical Methods in Engineering,* vol. 39, no. 15, pp. 2619 - 2633, 1996.

[23] G. Amarpuri, C. Zhang, C. Diaz, B. Opell, T. Blackledge and A. Dhinojwala, “Spiders Tune Glue Viscosity to Maximize Adhesion,” *ACS Nano,* vol. 9, no. 11, pp. 11472-11478, 2015.

[24] B. Opell, D. Jain, A. Dhinojwala and T. Blackledge, “Tuning orb spider glycoprotein glue performance to habitat humidity,” *Journal of Experimental Biology,* vol. 221, p. jeb161539, 2018.

[25] J. O. Wolff, G. B. Paterno, D. Liprandi, M. J. Ramírez, F. Bosia, A. Meijden, P. Michalik, H. M. Smith, B. R. Jones, A. M. Ravelo, N. Pugno and M. E. Herberstein, “Evolution of aerial spider webs coincided with repeated structural optimization of silk anchorages,” 2019.

[26] Tian, Yu, et al., “Adhesion and friction in gecko toe attachment and detachment.,” *Proceedings of the National Academy of Sciences,* vol. 103, no. 51, pp. 19320-19325, 2006.

[27] J. Wolff, I. Grawe, M. Wirth, A. Karstedt and G. SN., “Spider's super-glue: thread anchors are composite adhesives with synergistic hierarchical organization.,” *Soft matter,* vol. 11, no. 12, pp. 2394-2403, 2015.

[28] J. Wolff, D. Liprandi, F. Bosia and N. Pugno, “Robust substrate anchorages of stiff silk lines with extensible nano-fibres,” *in preparation.*